



HAL
open science

Chemical Composition of Lithiated Nitrodonickelates $\text{Li}_{3-xy}\text{Ni}_x\text{N}$: Evidence of the Intermediate Valence of Nickel Ions from Ion Beam Analysis and Ab Initio Calculations

Thomas Fernandes, Thomas Cavoué, P. Berger, Céline Barreteau,
Jean-Claude Crivello, Nicolas Emery

► To cite this version:

Thomas Fernandes, Thomas Cavoué, P. Berger, Céline Barreteau, Jean-Claude Crivello, et al.. Chemical Composition of Lithiated Nitrodonickelates $\text{Li}_{3-xy}\text{Ni}_x\text{N}$: Evidence of the Intermediate Valence of Nickel Ions from Ion Beam Analysis and Ab Initio Calculations. *Inorganic Chemistry*, 2023, 62 (39), pp.16013-16020. 10.1021/acs.inorgchem.3c02117. hal-04228615

HAL Id: hal-04228615

<https://hal.science/hal-04228615v1>

Submitted on 22 Nov 2023

HAL is a multi-disciplinary open access archive for the deposit and dissemination of scientific research documents, whether they are published or not. The documents may come from teaching and research institutions in France or abroad, or from public or private research centers.

L'archive ouverte pluridisciplinaire **HAL**, est destinée au dépôt et à la diffusion de documents scientifiques de niveau recherche, publiés ou non, émanant des établissements d'enseignement et de recherche français ou étrangers, des laboratoires publics ou privés.

Chemical composition of lithiated nitrodonickelates $\text{Li}_{3-x}\text{Ni}_x\text{N}$: evidence of the intermediate valence of nickel ions from ion beam analysis and *ab-initio* calculations.

Thomas Fernandes ¹, Thomas Cavoué ^{1,†}, Pascal Berger ², Céline Barreteau ¹, Jean-Claude Crivello ¹, Nicolas Emery ^{1,*}

¹ Univ Paris Est Creteil, CNRS, ICMPE, UMR 7182, 2 rue Henri Dunant, 94320 Thiais, France

² NIMBE, CEA, CNRS, Université Paris-Saclay, CEA Saclay, 91191 Gif sur Yvette Cedex, France

ABSTRACT

Lamellar lithiated nitridonickelates have been investigated from both experimental and theoretical points of view in a wide range of compositions. In this work, we evidence that the nickel ion in lamellar lithiated nitridonickelates adopts an intermediate valence close to +1.5. This solid-solution can therefore be written $\text{Li}_{3-1.5x}\text{Ni}_x\text{N}$ with $0 \leq x \leq 0.68$. Attempts to introduce more nickel into these phases systematically lead to the presence of the endmember of the solid solution, $\text{Li}_{1.97}\text{Ni}_{0.68}\text{N}$, with metallic nickel as impurity. The LiNiN phase has never been

observed and first-principles calculations suggested that all the structural configurations tested were mechanically unstable.

INTRODUCTION

The lamellar lithium nitride, Li_3N , and its transition metal substituted derivatives, the ternary lithium nitridometalates, attracted attention due to their ionic conductivity [1,2,3,4], electrochemical activities as Li-ion negative electrode materials [5,6,7,8,9], or hydrogen storage capabilities [10,11,12,13]. The structure of these lithiated transition metal nitrides is based on the hexagonal Li_3N structure-type (S.G. $P6/mmm$) shown in **Figure 1**. Nitrogen ions are in the $1a$ Wyckoff site, and lithium ions fill the $1b$ and $2c$ sites. Based on this compound, substitution is a traditional way to tune properties for specific applications. In Ni, Co or Cu derivatives, transition metal species substitute lithium ions located in the interplanar $1b$ site, and, depending on the oxidation state of the transition metal, lithium vacancies are created in the $2c$ site to compensate the charge difference.

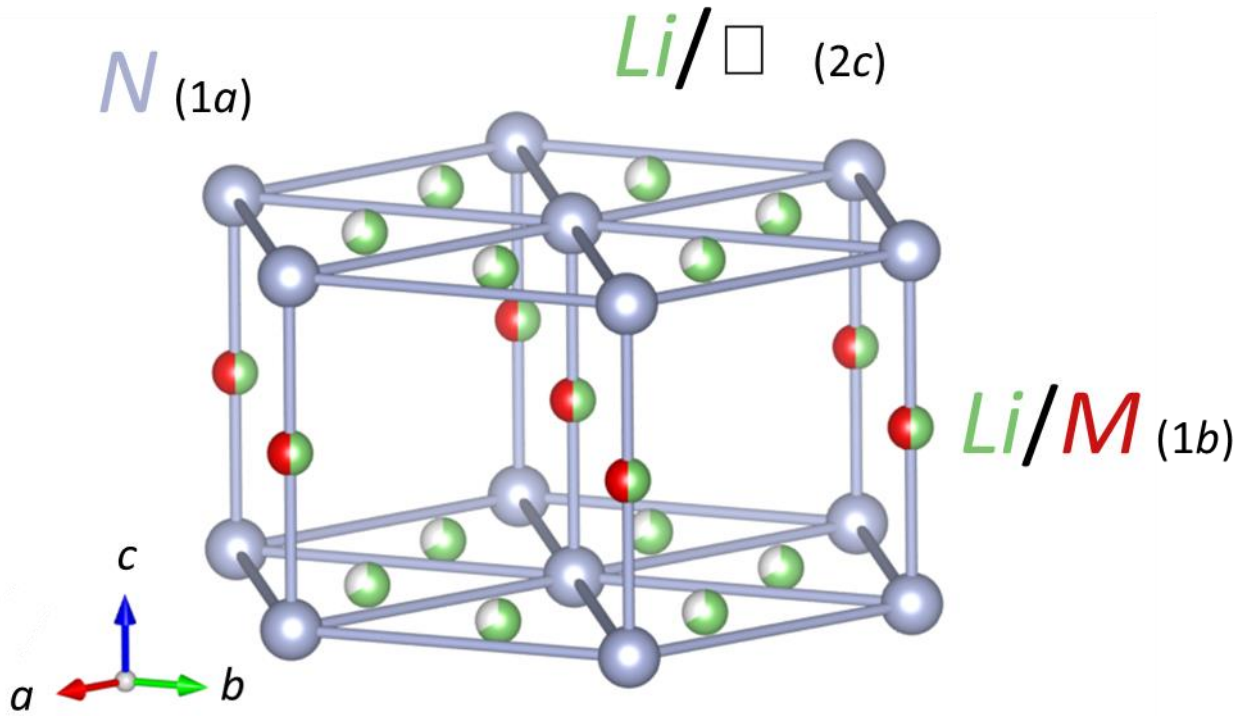
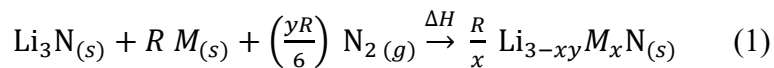


Figure 1: Li_3N -type hexagonal structure (S.G. $P6/mmm$) of $\text{Li}_{3-x}\text{M}_x\text{N}$ with $M=\text{Cu}$, Ni or Co .

These lamellar phases are usually prepared by reacting Li_3N with the transition metal in a nitrogen atmosphere at 580°C to 750°C [5,7,8,14,15]. Nitrogen acts as an oxidant in the reaction between Li_3N and the transition metal M ($M=\text{Co}$, Cu , Ni) which can be written:



where R is the molar ratio $R = M/\text{Li}_3\text{N}$, y is the transition metal oxidation state in $(\text{Li}^+)_{3-xy}(\text{M}^{y+})_x\text{N}^{3-}$ and x , the fraction of the transition metal M present in the $1b$ site. Thus, the final chemical composition is directly related to the nitrogen uptake required to oxidize the transition metal M^{y+} . In addition, the synthesis temperature around 700°C and higher under continuous nitrogen flow favors the lithium sublimation, which may lead to uncertainty in the lithium content. The literature suggests different oxidation states for the transition metal ions in these

phases, ranging from +1 degree [4,14,16,17,18,19] to +2 degrees [5,15,20, 21, 22,23,24,25], with some reports of intermediate valences [7,26,27,28].

Table 1 summarizes the oxidation states proposed for nitridonickelates prepared under different synthesis conditions. Such a dispersion in the reported compositions, and therefore, in the oxidation state of the nickel ions, could be attributed to the difficulty of simultaneously determining lithium, nickel and nitrogen contents. In this work we have prepared a series of $\text{Li}_{3-x}\text{Ni}_x\text{N}$ samples by a solid-state route under nitrogen flow. The composition was determined by two Ion Beam Analysis (IBA) methods: the Nuclear Reaction Analysis (NRA) and the Rutherford Backscattering Spectrometry (RBS). These methods are particularly suitable for determining the composition of light elements such as lithium and nitrogen simultaneously with transition metals. Measurements were carried out on bulk samples in order to gain insight into their homogeneity, thus allowing the composition to be correlated with the structural characterization carried out by X-Ray diffraction (XRD). In addition, a theoretical evaluation of the stability of several metal contents with 3 different oxidation states, i.e., +1, +1.5 and +2, was carried out by first principles calculations using the Special Quasi-random Structures (SQS) method to describe disordered cells.

Table 1: Composition, nickel oxidation state and synthesis conditions as reported in the literature.

Composition	Oxidation state	Synthesis condition	reference
LiNiN	+2	Li ₃ N on Ni foil 750°C 7days in N ₂ atm.	[6,24,25,28]
Li _{1.36} Ni _{0.79} N	+2	Li ₃ N in Ni tube 750°C 5 days in N ₂ atm.	[21]
Li ₅ Ni ₃ N ₃ (Li _{1.67} NiN)	+1.33	Li ₃ N in Ni tube 750°C 24h in N ₂ atm.	[28]
Li ₅ [(Li _{0.23} Ni _{0.77})N] ₃ (Li _{1.90} Ni _{0.77} N)	+1.43	Li ₃ N+Ni mixture under N ₂ rapid cooling from 900°C	[27]
Li _{3-2x} Ni _x N (0.2 ≤ x ≤ 0.6)	+2	Mixture Li ₃ N+Ni powders 700°C 8h under N ₂ flux	[5,20]
Li _{3-x} Ni _x N (0.0 ≤ x ≤ 0.85)	+1	Mixture Li ₃ N+Ni powders 500-600°C, 20-40h in N ₂ atm.	[17]
Li _{2.32} Ni _{0.36} N	+1.88	Li ₃ N on Ni foil 690°C, 7 days in N ₂ atm.	[26]
Li _{2.53} Ni _{0.34} N	+1.37	Li ₃ N on Ni foil 690°C, 24h in N ₂ atm.	[26]
Li _{2.48} Ni _{0.36} N	+1.45	Li ₃ N on Ni foil 580°C, 7 days in N ₂ atm.	[26]
Li _{2.0} Ni _{0.56} N	+1.73	Li ₃ N on Ni foil 690°C, 7 days in N ₂ atm.	[26]
Li _{2.2} Ni _{0.58} N	+1.32	Li ₃ N on Ni foil 580°C, 7 days in N ₂ atm.	[26]
Li _{1.63} Ni _{0.74} N	+1.84	Li ₃ N on Ni foil 690°C, 7 days in N ₂ atm.	[26]
Li _{2.0} Ni _{0.67} N	+1.5	Mixture Li ₃ N+Ni powders 720°C 12h under N ₂ flux	[7]

EXPERIMENTAL AND COMPUTATIONAL DETAILS

Lithiated nitridonickelates of the solid solution $\text{Li}_{3-x}\text{Ni}_x\text{N}$ were prepared by solid-state synthesis in a nitrogen atmosphere from Li_3N and metallic nickel powder. Due to the moisture-sensitive nature of lithium nitride and its derivatives, all manipulations were performed in an Ar-filled gloves box ($p(\text{H}_2\text{O}) < 0.1$ ppm, $p(\text{O}_2) < 0.1$ ppm). Mixtures of Li_3N (Alfa Aesar, 99.4% metal basis) and metallic nickel powders with different Ni/ Li_3N molar ratios were prepared, thoroughly ground in an agate mortar and then die pressed into a pellet (13mm diameter). After being placed in an alumina crucible, the sample was transferred into a specially designed stainless-steel reactor, which allowed thermal treatment at 720 °C under continuous N_2 flow for 12 h. To trap possible traces of oxygen in nitrogen gas, the sample was surrounded by crucibles filled with titanium sponge.

X-ray diffraction patterns were collected with a Panalytical X'Pert Pro diffractometer using cobalt radiation and equipped with an X'celerator rapid detector. The GSAS+EXPGui package was used to analyze the diffraction patterns by the Rietveld method [29,30]. Powder samples were kept under argon during the acquisition using an airtight polymer sample holder.

Quantitative analysis of nickel in as-prepared samples was performed by complexometric titration with EDTA in basic media using Murexide as a colored indicator. The powder was mineralized with a nitric acid solution and then the pH was adjusted to 9 by adding NH_4OH (30%) solution. In addition, the complete chemical composition was determined by ion beam analysis (IBA), including Rutherford backscattering (RBS) and nuclear reaction analysis (NRA). The IBA experiments were performed with a 3.03 MeV H^+ beam produced by the Van de Graaf accelerator of IRAMIS/LEEL at CEA-Saclay. The spectrum was collected with an annular detector covering backscattering angles centered around 170°. The collected spectra were analyzed using the SimNRA software [31]. The following cross sections were used:

- Lithium: ${}^7\text{Li}(p,\alpha){}^4\text{He}$ nuclear reaction (energy of surface α 7 478 keV, measured at Saclay) [32], ${}^6\text{Li}(p,p_0){}^6\text{Li}$ [33], ${}^7\text{Li}(p,p_0){}^7\text{Li}$ [34] and ${}^7\text{Li}(p,p_1){}^7\text{Li}$ [35] for elastic scattering
- Nitrogen: ${}^{14}\text{N}(p,p_0){}^{14}\text{N}$ elastic scattering [36]
- Nickel: Rutherford cross sections of Ni isotopes

For the computational part, electronic calculations were performed in the framework of the Density Functional Theory (DFT). The Li-Ni-N system has been considered in several crystal structures depending on the composition. A complete study of the $\text{Li}_{3-1.5x}\text{Ni}_x\text{N}$ compounds has been performed in the hexagonal $P6/mmm$ space group as described in **Figure 1**. The endmember Li_3N has been built by a full occupation of Li on both the $1b$ and $2c$ sites. The hypothetical LiNiN compound has been studied considering several possible symmetries ($P6m2$, $P62m$ [24], $P6_3/mmc$ or $P4_2/mmc$ [37]). Schematic representations and cell parameters are summarized in S.I.1 and 2 respectively. Disordered structures were generated for the Ni-substituted in the $P6/mmm$ space group using the Special Quasi-random Structure (SQS) method [38]. The cluster expansion formalism as implemented in the MCSQS algorithm provided in the Alloy-Theoretic Automated Toolkit (ATAT), was considered for the SQS cell generation [39]. According to the y -Ni valence considered on $(\text{Li}^+)_{3-xy}(\text{Ni}^{y+})_x\text{N}^{3-}$, the supercells were modelled by substituting Li/Ni and Li/vacancy at $1b$ and $2c$ sites respectively. For a given cell size N , the atomic distribution was chosen by minimizing the difference on correlation functions ζ_i for a set of clusters i with those of ideal randomized structure (estimated by the root mean square error, RMSE). In this study, the set of clusters considered was composed of the first 8 nearest-neighbor pairs (atomic distance less than 5.2 Å), the first 4 triangles (4.2 Å) and 2 tetrahedra (3.8 Å). By minimizing the sum of the RMSE of all considered ζ_i , supercells for a given N with a total number of atoms up to 188 were generated according to **Table 2**.

Table 2: Details of atomic numbers in the SQS supercell of $(\text{Li}^+)_{3-xy}(\text{Ni}^{y+})_x\text{N}^{3-}$.

	x_{Ni}	Li	Ni	N	Vacancies	N , Total Positions	Number of atoms	best RMSE (ζ_i)
Li_3N	0	3	0	1	0	4	4	
$\text{Li}_{2.76}\text{Ni}_{0.16}\text{N}$	0.167	132	8	48	4	192	188	0.12
$\text{Li}_{2.5}\text{Ni}_{0.33}\text{N}$	0.333	75	10	30	5	120	115	0.18
$\text{Li}_{2.25}\text{Ni}_{0.5}\text{N}$	0.500	45	10	20	5	80	75	0.27
$\text{Li}_2\text{Ni}_{0.66}\text{N}$	0.667	30	10	15	5	60	55	0.35
LiNiN	1	1	1	1	0	3	3	

The DFT calculations were performed using the Vienna Ab Initio Simulation Package (VASP) [40,41] with the Generalized Gradient Approximation (GGA) and the Perdew-Burke-Ernzerhof (PBE) functional [42]. The energy cutoff was set at 600 eV, considering the spin polarization, and a dense grid of k-points with a spacing of less than 0.05 Å was generated using the Monkhorst-Pack procedure [43]. The internal atomic coordinates and lattice parameters were relaxed to ensure a convergence of Hellmann-Feynman forces better than 1 meV/Å, and the total energy calculations converged to less than 0.1 meV. The density of states (DOS) was calculated using the linear tetrahedron method with Blöchl corrections on the relaxed structures. Only the electronic contributions to the heats of formation and reaction at 0 K were considered. The charge distribution on the atoms was analyzed using Bader’s topological analysis, which divides space into atomic regions with minimum charge density surfaces. The Bader code developed by Henkelman *et al.* was used for this purpose [44]. In the framework of the frozen phonons method [45], the harmonic lattice stability was estimated on supercells of ordered structures with relevant atomic displacements generated by the Phonopy code [46].

RESULTS

A series of lithiated nitridonickelates were prepared with various Ni/Li₃N molar ratios between 0 and 1.1. For Ni/Li₃N ratios higher than 1, metallic nickel was identified in the XRD diffraction pattern, indicating an incomplete reaction of nickel powder with Li₃N (**Figure 2**). All the obtained diffraction patterns were easily indexed using a hexagonal cell within the *P6/mmm* space group. A small diffraction peak around 39° was observed, attributed to Li₂O. For R = 1.1, additional diffraction peaks at 52.2° and 91.7° clearly indicate the presence of an additional secondary phase, metallic nickel. Thus, the maximum nickel content is reached at a molar ratio Ni/Li₃N lower than 1.1.

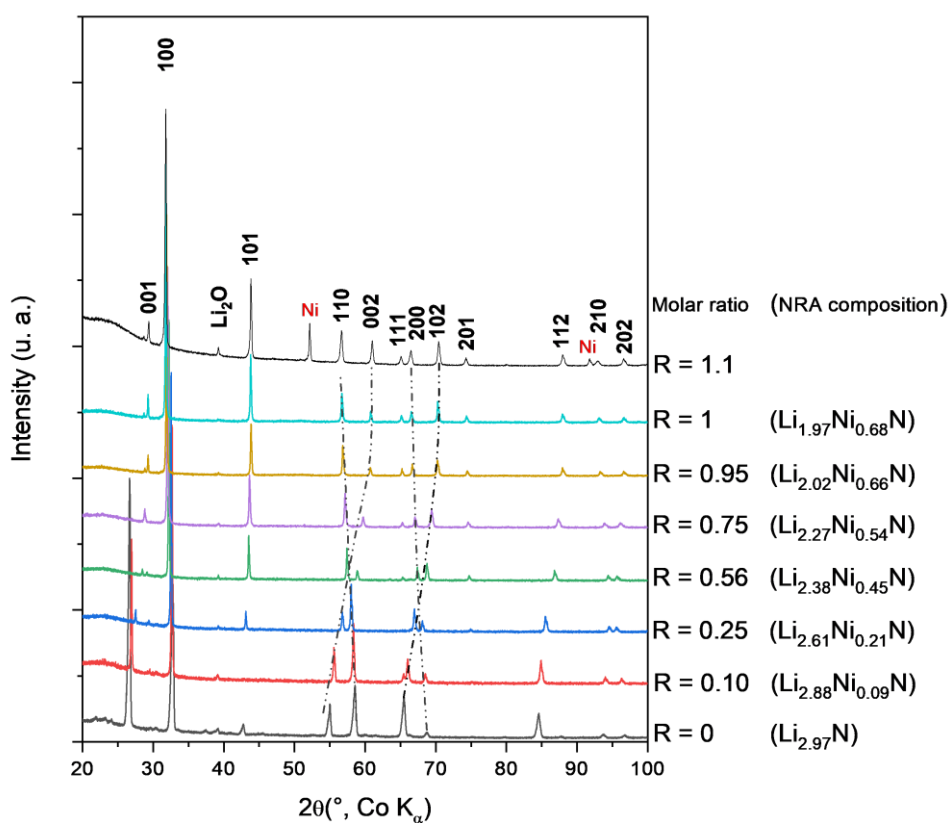


Figure 2: XRD patterns obtained for various Ni/Li₃N initial molar ratios *R*.

Composition determined by NRA are reported into brackets.

A continuous shift to the higher angles is observed for diffraction peaks related to the *c*-axis, indicating a gradual contraction of the interlayer distance with increasing nickel content.

Conversely, the $hk0$ peaks gradually shift to the lower angles, consistent with a contraction of the a cell parameter. These observations agreed with the solid solution behavior of this system observed elsewhere [5,17,25]. The cell parameters were accurately determined from the XRD patterns using the Rietveld method. **Figure 3** shows an example of the refined XRD pattern of a sample obtained after reaction of metallic nickel powder with Li_3N powder in a ratio $\text{Ni}/\text{Li}_3\text{N} = 0.75$. These analyses confirm the substitution of lithium ions by nickel ions at site $1b$. However, due to its low atomic number, lithium is almost transparent to X-rays. Thus, XRD methods are not suitable to refine the site occupancies within the structure. Therefore, accurate determination of the sample is essential to plot the evolution of cell parameters with the nickel content.

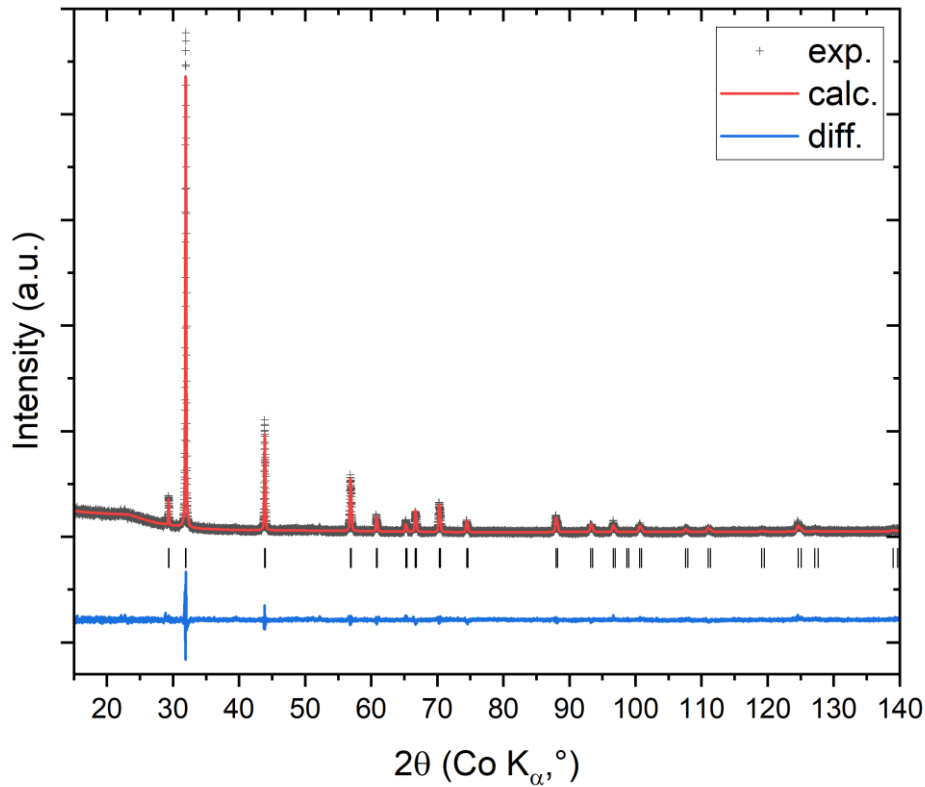


Figure 3: XRD pattern fitted within the Rietveld method for the sample prepared with an initial molar ratio $R_{\text{Ni/Li3N}}=0.75$ (composition of $\text{Li}_{2.27}\text{Ni}_{0.54}\text{N}$). “+” symbols are experimental data; red line is the calculated pattern and blue line is the difference line. “|” markers indicate the diffraction peaks of the hexagonal cell within the $P6/mmm$ space group.

As mentioned above, IBA methods allow the simultaneous determination of the lithium, nitrogen, and nickel contents of the sample. The homogeneity of the sample can be checked on the μm scale. The sample prepared with a molar ratio $R = 1.1$ was not measured due to the presence of unreacted nickel. An example of the IBA spectrum recorded for is shown in **Figure 4a**. Below 3 MeV different contributions are observed corresponding to the RBS signals of nickel (purple line), nitrogen (blue line) and lithium (green line). The black line corresponds to

the sum of these three contributions. It should be compared with the experimental data plotted by the red dots.

The two asterisked peaks at 2.17 and 2.59 MeV represent carbon and oxygen contributions respectively. The shape of these signals, i.e., sharp small peaks, suggests the formation of a few nanometers thick layer at the surface containing these elements and not a bulk distribution in the sample [47]. Conversely, the edges of the nitrogen and nickel are slightly smoothed, indicating a depletion of these elements at the surface. Both observations are the signature of the surface degradation during the air transfer into the chamber analysis and are consistent with the moisture sensitive nature of lithiated transition metal nitrides [48,49]. Similar observations have been made during analyses of air sensitive graphite intercalation compounds [50,51].

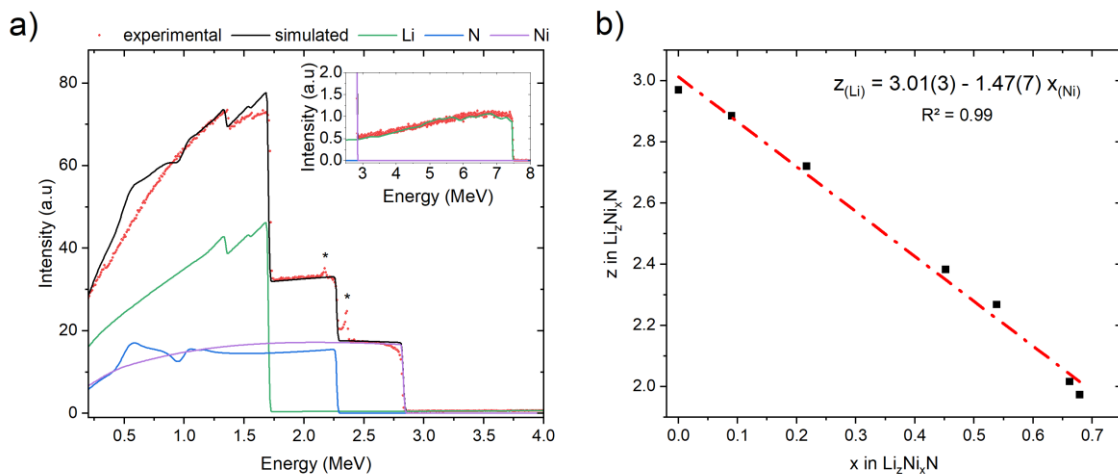


Figure 4: (a) IBA spectrum of $\text{Li}_{2.27}\text{Ni}_{0.54}\text{N}$ ($R_{\text{Ni}/\text{Li}_3\text{N}}=0.75$) RBS part of the spectrum correspond to the energy lower than incident energy (3.0 MeV) and NRA part to the higher energies. (b) z in $\text{Li}_z\text{Ni}_x\text{N}$ as a function of x in $\text{Li}_z\text{Ni}_x\text{N}$. the slope of the linear regression corresponds to the opposite of the nickel oxidation state.

Figure 4b shows the evolution of Li content as a function of Ni content, with nitrogen content fixed at 1 for each phase. As expected, the lithium fraction gradually decreases with increasing

nickel content, from 2.97 for the Ni-free sample to 1.97 for the nickel-richest single-phase sample (Ni = 0.68). According to the general chemical formula $\text{Li}_{3-xy}\text{Ni}_x\text{N}$, the lithium content z depends on x , the nickel content, and y , the oxidation state of the nickel ions. The linear regression in **Figure 4b** indicates that the nickel ions adopt the same oxidation state under our synthesis conditions and over the entire range of the nickel content in the solid-solution. The slope of the linear correlation indicates an average oxidation state of 1.47(7). Thus, nickel ions are in an intermediate valence state.

Table 3: Experimental cell parameters for $\text{Li}_{3-1.5x}\text{Ni}_x\text{N}$.

$\text{Li}_{3-1.5x}\text{Ni}_x\text{N}$ ($R\text{Ni}/\text{Li}_3\text{N}$)	Cell parameter (Å)		Ratio c/a
	a	c	
Li_3N ($R = 0$)	3.656	3.872	1.06
$\text{Li}_{2.86}\text{Ni}_{0.09}\text{N}$ ($R = 0.1$)	3.668	3.832	1.04
$\text{Li}_{2.688}\text{Ni}_{0.208}\text{N}$ ($R = 0.25$)	3.690	3.765	1.02
$\text{Li}_{2.32}\text{Ni}_{0.45}\text{N}$ ($R = 0.56$)	3.725	3.641	0.98
$\text{Li}_{2.19}\text{Ni}_{0.538}\text{N}$ ($R = 0.75$)	3.739	3.589	0.96
$\text{Li}_{2.00}\text{Ni}_{0.66}\text{N}$ ($R = 0.95$)	3.756	3.541	0.94
$\text{Li}_{1.97}\text{Ni}_{0.68}\text{N}$ ($R = 1$)	3.762	3.532	0.94
“ $\text{Li}_{1.97}\text{Ni}_{0.68}\text{N} + \text{Ni}$ ” ($R = 1.1$)	3.772	3.528	0.94

Table 3 summarizes the experimental cell parameters with their composition determined by IBA analysis. The cell parameters a and c evolve linearly with the nickel content: a gradually

increases with the nickel content from 3.656 Å for the nickel-free sample to 3.762 Å for $\text{Li}_{1.97}\text{Ni}_{0.68}\text{N}$. On the other hand, c decreases linearly with increasing nickel content from 3.872 Å to 3.531 Å for Li_3N and $\text{Li}_{1.97}\text{Ni}_{0.68}\text{N}$, respectively. These overall trends are in good agreement with the analysis performed using the empirical Bond Valence Sum approach (S.I.3, [52,53]). The $\text{Li}_{3-yx}\text{Ni}_x\text{N}$ cell parameters of the sample containing metallic nickel as an impurity ($R=1.1$) were added for comparison. Thus, cell parameter values of the latter are very close to those of the $\text{Li}_{1.97}\text{Ni}_{0.68}\text{N}$ sample ($R=1$), suggesting that the endmember of the solid solution contains about 0.68 Ni per unit formula.

In parallel with the experimental investigations, theoretical calculations were carried out to confirm the experimental results. Our first investigation was dedicated to the influence of the transition metal valence y^+ on the phase stability in the lithium nitrides $(\text{Li}^+)_{3-yx}(\text{M}^{y+})_x\text{N}^{3-}$ substituted by Ni or Cu. The transition metal oxidation state in M^{y+} was tuned by adjusting the x composition in a SQS supercell, assuming the Li and N charges to be +1 and -3 respectively. Thus, SQS calculations allowed the generation of supercell corresponding to a Ni-substituted disordered structure (the same for Cu), DFT calculations gave the enthalpy of formation for each possible valence. For Ni and Cu, 3 possible y valences, +1, +1.5 and +2, were tested in $\text{Li}_y\text{M}_{0.33}\text{N}$ ($M = \text{Cu}$ or Ni) and the variation of the enthalpy of formation function of the valence are reported in **Figure 5**. The enthalpy of formation for both Cu and Ni has a minimum corresponding to the optimal valence, Cu^{1+} and $\text{Ni}^{1.5+}$, as shown by the line drawn for the eye. Therefore, the Cu^{1+} valence is the most stable configuration, according to the $\text{Li}_{3-x}\text{Cu}_x\text{N}$ compositions reported in the literature [9,14 ,16 ,17].

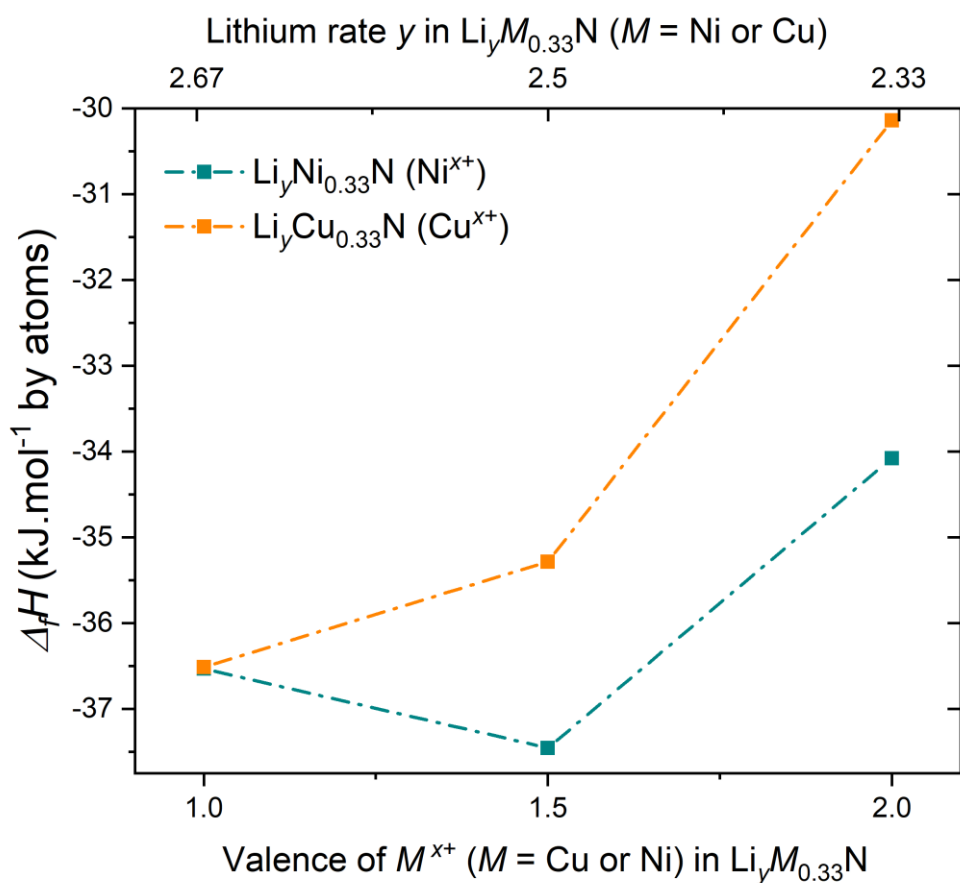


Figure 5 : Evolution of the enthalpy of formation as function of the valence of Ni or Cu in $\text{Li}_y\text{M}_{0.33}\text{N}$ ($M = \text{Ni or Cu}$)

According to this first result on the Ni phase with a most stable valence at +1.5, all compounds from the solid solution $\text{Li}_{3-1.5x}\text{Ni}_x\text{N}$ were calculated considering Ni as $\text{Ni}^{1.5+}$. The enthalpies of formation obtained from the DFT calculations are shown in **Figure 6** as function of Ni content. All the enthalpies of formation are negative and behave continuously in the same range around -35 to -40 kJ mol^{-1} . In **Figure 6** the enthalpy of formation of LiNiN is also added. The resulting value is quite different, jumping from the other values of the solid solution by a 25 kJ mol^{-1} step. The reported value is related to the $P-6m2$ structure, which was found to be the most stable structure evaluated in this work (with the lowest enthalpy value, S.I. 2). This result suggests that LiNiN is less stable than the intermediate valence solid solution compositions $\text{Li}_{3-1.5x}\text{Ni}_x\text{N}$.

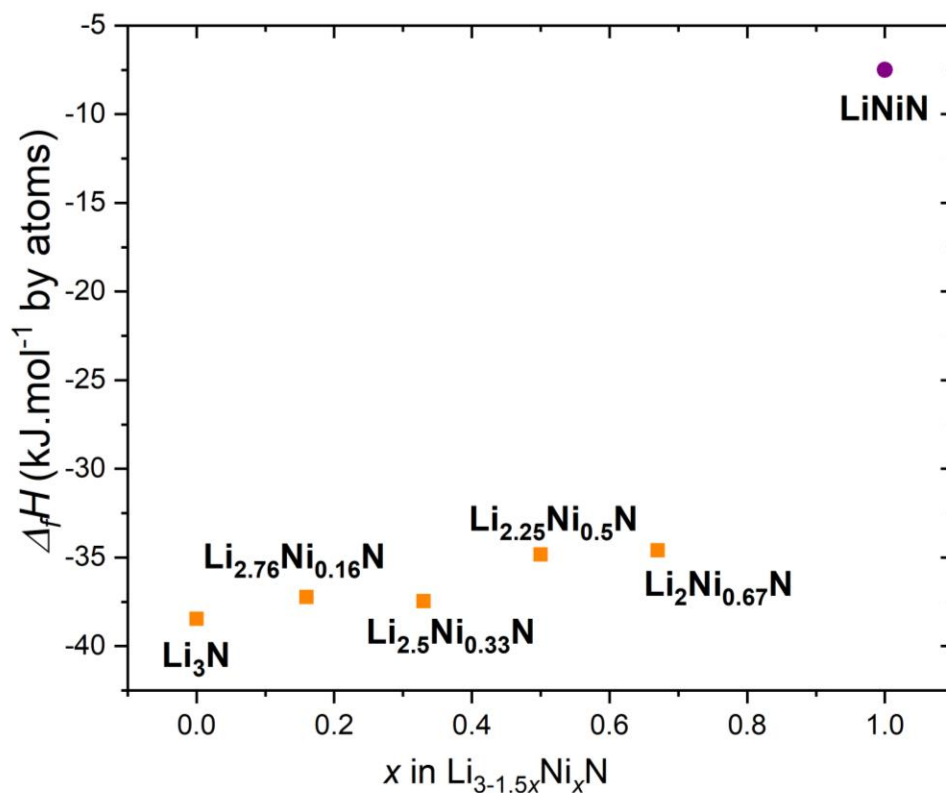


Figure 6: Calculated enthalpy of formation as function of the Ni content x in $\text{Li}_{3-1.5x}\text{Ni}_x\text{N}$ and LiNiN

The calculated cell parameters of all the Ni solid solution compounds are summarized in **Table 4**. It can be noticed that increasing Ni content, leads to the appearance of magnetic moments in the structure. The evolution of the Bader charges with the Ni content suggests a decrease in the ionic character of both Li-N and Ni-N bonds: the net charge of both Li and N decreases significantly.

Table 4: DFT results for $\text{Li}_{3-1.5x}\text{Ni}_x\text{N}$ (cell parameter, enthalpy of formation, magnetic moment, and Bader charges).

	Cell parameters (Å)		Enthalpy of formation ($\text{kJ}\cdot\text{mol}^{-1}\cdot\text{at}^{-1}$)	Magnetic Moment ($\mu\text{B}\cdot\text{at}^{-1}$)	Bader charges (Li)	Bader charges $\gamma(\text{N})$	Bader charges $\gamma(\text{Ni})$
	<i>a</i>	<i>c</i>					
Li_3N	3.639	3.871	-38.45	0.0	0.796	-2.389	
$\text{Li}_{2.76}\text{Ni}_{0.16}\text{N}$	3.616	3.796	-37.23	0.042	0.736	-1.983	-0.252
$\text{Li}_{2.5}\text{Ni}_{0.33}\text{N}$	3.668	3.714	-37.45	0.061	0.808	-2.015	-0.012
$\text{Li}_{2.25}\text{Ni}_{0.5}\text{N}$	3.680	3.625	-34.84	0.087	0.515	-1.240	0.164
$\text{Li}_2\text{Ni}_{0.67}\text{N}$	3.684	3.551	-34.61	0.018	0.398	-0.920	0.187
LiNiN (<i>P-6m2</i>)	3.637	3.415	-7.50	0.0	0.841	-1.147	0.3026

DISCUSSION

As described in the results section, the IBA experiments indicate that the nickel ions adopt an intermediate valence of +1.5 throughout the solid-solution $\text{Li}_{3-yx}\text{Ni}_x\text{N}$ composition range. Such a result is consistent with the enthalpy of formation calculated for several valences y of the $\text{Li}_{3-y/3}\text{Ni}_{0.33}\text{N}$ compositions, which has a minimum for an intermediate valence $\text{Ni}^{1.5+}$. This statement is not sufficient to argue that the compound is stable with respect to other phases in the ternary system. However, it is a strong indication that this is the more stable hypothesis and supports the value confirmed by the literature. For comparison, the case of $M = \text{Cu}$ was also calculated and for this transition metal ion, the minimum corresponds to the valence = +1. Thus, for lithiated copper nitrides, such a valence implies an absence of lithium vacancies in the $2c$ site while a fraction of the $1b$ site is filled by the copper ions [9,14,16,17]. Therefore, lithium substitution by copper in the $1b$ site does not change the composition of the Li_2N^- layer. In addition, Li^+ and Cu^+ ions have a similar ionic radius [54]. With an almost constant a value and

a slight decrease of the c parameter, it is in good agreement with the cell parameter evolutions of the $\text{Li}_{3-x}\text{Cu}_x\text{N}$ solid solution [9].

The cell parameters obtained from XRD measurements and those calculated by DFT for the SQS supercells as a function of the Ni content in $\text{Li}_{3-1.5x}\text{Ni}_x\text{N}$ are shown in **Figure 7**. Both experimental and theoretical values behave similarly with a remarkable agreement for the c parameter. The calculated value of c for Li_3N , 3.871 Å, is in perfect agreement with the experimental value (3.872 Å). Experimentally, the substitution of some Li^+ ion by $\text{Ni}^{1.5+}$ in the $1b$ site induces a linear decrease of the c parameter, from 3.872 Å for Li_3N to 3.762 Å for $\text{Li}_{1.97}\text{Ni}_{0.68}\text{N}$, with a slope of $-0.508(9) x_{\text{Ni}}$. Theoretical data replicate this trend well with a slope of $-0.484(8) x_{\text{Ni}}$, resulting in a negligible discrepancy for the richest calculated Ni composition, $\text{Li}_2\text{Ni}_{0.67}\text{N}$, of ~ 0.02 Å. A larger discrepancy is seen for the in-plane cell parameter a . The computed Li_3N a parameter is slightly underestimated at 3.639 Å compared to the experimental value of 3.656 Å. Such a small difference in the a parameter while the c parameter is accurately reproduced has already been observed previously [55]. Increasing the nickel content, and then the lithium vacancy in the $2c$ site, induces a gradual increase in of the a parameter. If the experimental evolution is a clear straight line with a slope of $0.154x$, the calculated values increase with a smaller slope of $0.092x$ and a wider dispersion than for the c -axis parameter. Such a dispersion may be due to the complexity of describing the random distribution of the $\text{Ni}^{1.5+}$ ion in the $1b$ site and of the vacancy in the $2c$ site. However, the deviation is limited to 2% and there is a striking agreement between the calculations and the experimental results. These results confirm the existence of the complete solid solution for $x \leq 0.68$ since no slope break is observed for either cell parameter. In addition, the enthalpies of formation for the solid solution compounds are close to those of Li_3N , with a slight increase with the nickel content (**Figure 6**).

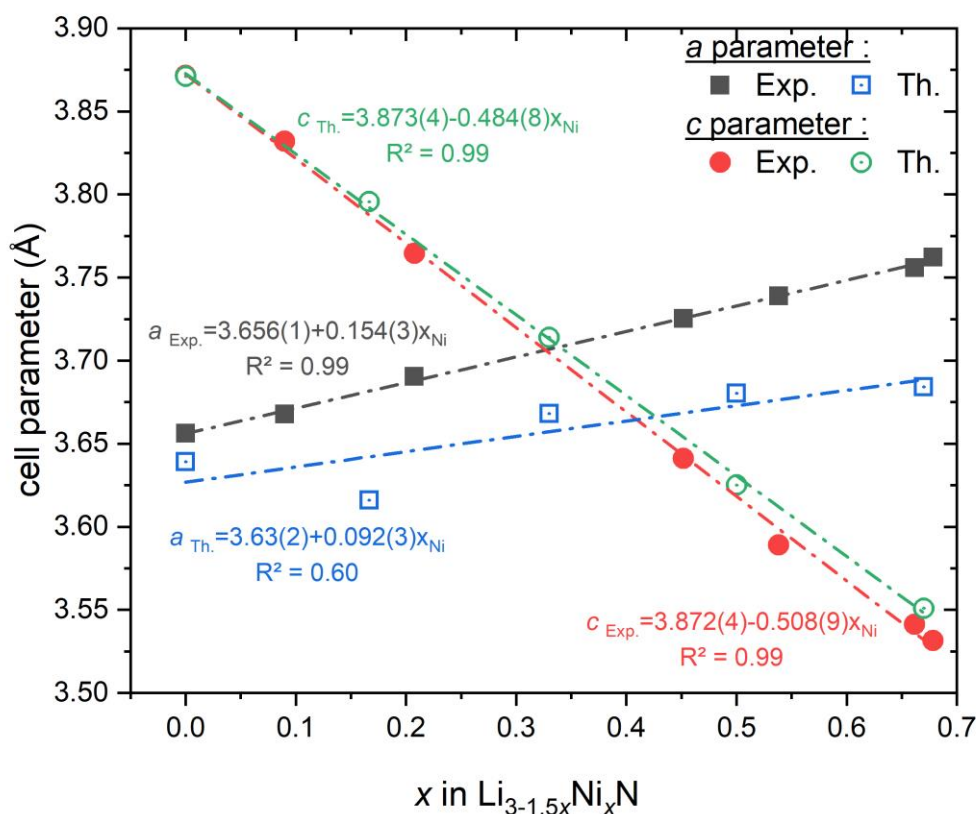
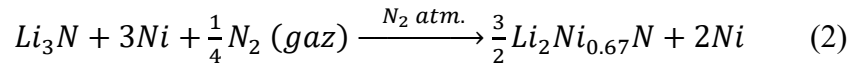


Figure 7: cell parameters of $\text{Li}_{3-1.5x}\text{Ni}_x\text{N}$ as a function of the nickel content. Solid symbols represent experimental parameters, open symbols correspond to theoretical values (DFT calculations).

Several experimental reports claim the existence of the Ni-rich phase LiNiN [6,24,25]. However, under our synthesis conditions, this phase was not observed, even as a by-product. As mentioned earlier in this paper, for Ni/ Li_3N ratios greater than 1, metallic nickel is observed as a secondary phase in addition to $\text{Li}_{1.97}\text{Ni}_{0.68}\text{N}$, the endmember of the solid solution. Therefore, we have performed a computational analysis of LiNiN with the reported structure ($P-6m2$ structure [24]) and with several alternative structures (space groups $P-62m$, $P6_3/mmc$, or $P4_2/mmc$). These results suggest that LiNiN is not stable. In fact, even if a negative value for the enthalpy of formation has been found for all the hexagonal structures (the orthorhombic cell

proposed in [37] has a positive enthalpy of formation, S.I. 2), these values are 4 times smaller compared to the other lamellar Li-Ni-N solid solution phases. Moreover, in contrast to the $\text{Li}_{3-1.5x}\text{Ni}_x\text{N}$ phases, the calculated cell parameters are far from the reported experimental cell parameters ($a_{\text{th}} = 3.637 \text{ \AA}$ and $c_{\text{th}} = 3.415 \text{ \AA}$ instead of $a = 3.74304(5) \text{ \AA}$ and $c = 3.52542(6) \text{ \AA}$ [24]). It is worth noting that the experimental values reported in [24] are close to those obtained from both experimental and computational values of the nickel-richest composition $\text{Li}_{1.98}\text{Ni}_{0.68}\text{N}$ studied in this work. From the electrochemical performance point of view, both LiNiN [6] and $\text{Li}_2\text{Ni}_{0.67}\text{N}$ [7] show a stable specific capacity of 200 mAh g^{-1} in the 0 - 1.3 V potential window. Then, all these results suggest that LiNiN is not stable and decomposes into $\text{Li}_2\text{Ni}_{0.67}\text{N}$ plus Ni metal as reported by XRD measurements presented in previous sections.



Additional phonon calculations were performed to confirm or not the stability of the LiNiN composition. However, regardless of the structural model chosen (S.I.4), this compound is mechanically unstable since negative frequencies are systematically observed.

Having shown that the LiNiN compound is not stable, we can now discuss the evolution of the electronic charge transfer in the $\text{Li}_{3-x}\text{Ni}_x\text{N}$ solid solution for $x < 1$. Indeed, changes as a function of the substitution rate x are observed as shown in **Table 4**. The Bader charge estimate of Li starts at +0.8 for Li_3N and drops to +0.4 for the $x = 0.67$ compound. The charge of nitrogen is also strongly affected from -2.4 to -1. This behavior indicates a shift from ionic to covalent bonds. According to previous study in the dilute limit ($\text{Li}_{3-x-y}\text{M}_x\text{N}$ with $x < 2\%$ and $\text{M} = \text{Co}, \text{Ni}, \text{Cu}$, [56]), substituting lithium in the $1b$ site with Ni lowers the band gap to 0.55 eV due to the covalent nature of the Ni-N bonds. Our preliminary studies of the calculated density of states (DOS) of the compounds in solid solution show that the band gap of Li_3N cancels with larger Ni, leading to the presence of bands at the Fermi level. As shown in (S.I.5), Li_3N is

paramagnetic and has a band gap of about 1 eV, whereas all the other solid solution compounds are magnetic. Furthermore, if there is still a band gap in one spin direction and a small population at the Fermi level in the other direction for $x = 0.33$ (which is the expected percolation threshold for a triangular lattice), the compound is fully metallic for $x = 0.67$. Further work discussing the calculated electronic structure and the measured ionic conductivity is in progress and will be presented in an additional article.

CONCLUSION

We have studied the Li-Ni-N solid solution system using IBA, XRD and DFT calculations. A series of samples with different nickel contents were prepared from metallic nickel and lithium nitride powders by solid state synthesis under nitrogen flow. A theoretical analysis was also carried out using different supercells generated by the SQS approach to account for the random distribution of both the Ni ion in the $1b$ site and the lithium vacancies in the $2c$ site of the Li_3N type structure. Both experimental and theoretical results suggest an intermediate valence of +1.5 for the nickel ion throughout the solid solution domain. The maximum experimentally observed nickel content of these $\text{Li}_{3-1.5x}\text{Ni}_x\text{N}$ compounds is ~ 0.68 . Additional computational effort has been devoted to the Ni-rich composition LiNiN reported experimentally in [6,24,25]. This study, coupled with experimental evidence such as cell parameters or electrochemical capacity, suggests that LiNiN is not a stable and should lead to a segregation between $\text{Li}_{1.97}\text{Ni}_{0.68}\text{N}$ and metallic nickel.

Associated Content

Supporting Information Available:

S.I. 1: Schematic representation of the various LiNiN structural models evaluated theoretically; S.I. 2: Cell parameters and Enthalpy of formation for LiNiN

calculated in several prototypes; S.I.3: Bond Valence Sum analysis of $\text{Li}_{3-x}\text{Ni}_x\text{N}$ solid solution phases; S.I.4: Phonon dispersion curves for LiNiN within the 4 structures evaluated. S.I.5. Electronic density of states of $\text{Li}_{3-x}\text{Ni}_x\text{N}$ solid solution phases.

The Supporting Information is available free of charge on the ACS Publications website.

AUTHOR INFORMATION

Corresponding Author

* nicolas.emery@cnrs.fr

Present Address

† T. Cavoué, CEA-Liten, 17 rue des martyrs, 38054 Grenoble Cedex, France

Author Contributions

The manuscript was written through contributions of all authors. All authors have given approval to the final version of the manuscript.

Acknowledgements

DFT calculations were performed using HPC resources from GENCI-CINES (Grant A0060906175). All the Van de Graff accelerator support team at CEA Nimbe is acknowledge for their valuable technical assistance. ICMPE is acknowledge for financial support through the Transverse Project call.

References

-
- ¹ von Alpen, U.; Rabenau, A.; Talat, G. H.; Ionic conductivity in Li_3N single crystals, *Appl. Phys. Lett.* 1977, 30, 621-623
- ² Boukamp, B. A.; Huggins, R.A.; Lithium ion conductivity in lithium nitride, *Phys. Lett. A* 1976, 58, 231-233
- ³ Li, W.; Wu, G.; Araujo, C.M.; Scheicher, R.H.; Blomqvist, A.; Ahuja, R.; Xiong, Z.; Feng, Y.; Chen, P.; Li^+ conductivity and diffusion mechanism in $\alpha\text{-Li}_3\text{N}$ and $\beta\text{-Li}_3\text{N}$, *Energy Environ. Sci.*, 2010, 1524-1530
- ⁴ Powell, A.S.; Stoeva, Z.; Smith, R.I.; Gregory, D.H.; Titman, J.J.; Structure Stoichiometry and transport properties of lithium copper nitride battery materials: combine NMR and power neutron diffraction studies, *Phys. Chem. Chem. Phys.*, 2011, 13,10641-10-647
- ⁵ Ducros, J.B.; Bach, S.; Pereira-Ramos, J.P.; Willmann, P., A novel lithium intercalation compound based on the layered structure of lithium nitridonickelates $\text{Li}_{3-2x}\text{Ni}_x\text{N}$, *Electrochim. Acta* 2007, 52, 7035-7041
- ⁶ Cabana, J.; Stoeva, Z.; Titman, J.J.; Gregory, D.H.; Palacin, R, Toward new electrode materials for Li-ion batteries: Electrochemical properties of LiNiN , *Chem. Mater.* 2008, 20, 1676-1678
- ⁷ Cavoué, T; Emery, N; Umirov, N. ; Bach, S.; Berger, P.; Bakenov, Z.; Cénac-Morthe, C.; Pereira-Ramos, J.P., $\text{Li}_{2.0}\text{Ni}_{0.67}\text{N}$, a promising negative electrode material for Li-ion batteries with a soft structural response, *Inorg. Chem.* 2017, 56, 13815-13821
- ⁸ Nishijima, M.; Kagohashi, T.; Imanishi, M.; Takeda, Y.; Yamamoto, O.; Kondo, S. Synthesis and electrochemical studies of new anode material, $\text{Li}_{3-x}\text{Co}_x\text{N}$, *Sol. St. Ionics*, 1996, 83, 107-111
- ⁹ Bach, S.; Pereira-Ramos, J.P.; Ducros, S.; Willmann, P.; Structural and electrochemical properties of layered lithium nitridocuprates $\text{Li}_{3-x}\text{Cu}_x\text{N}$, *Solid Stat. Ionics*, 2009, 180, 231-235
- ¹⁰ Zhang, J.; Cerny, R.; Villeroy, B.; Godart, C.; Chandra, D.; Latroche, M.; $\text{Li}_{3-x}\text{M}_x\text{N}$ (M=Co, Ni) synthesized by Spark Plasma Sintering for hydrogen storage, *J. All. Com.*, 2011, 509S, S732-S735
- ¹¹ Gregory, D.H.; Lithium nitrides, imides and amides as lightweight, reversible hydrogen stores, *J. Mat. Chem.*, 2008, 18, 2321-2330
- ¹² Chen, P.; Xiong, Z.; Luo, J.; Lin, J.; Lee Tan, K.; Interaction of hydrogen with metal nitrides and imides, *Nature*, 2002, 420, 302-304
- ¹³ Ma, L.-P.; Wang, P.; Dai, H.-B.; Kong, L.-Y.; Cheng, H.-M.; Enhanced H-storage properties in Li-Co-N-H system by promoting ion migration, *J. All. Com.*, 2008, 466, L1-L4
- ¹⁴ Gordon, A. G.; Gregory, D. H.; Blake, A. J.; Weston, D. P.; Jones, M. O.; Ternary lithium nitridocuprates, $\text{Li}_{3-x-y}\text{Cu}_x$: crystal growth, bulk synthesis, structure and magnetic properties, *Int. J. Inorg. Mat.*, 2001, 3, 973-981
- ¹⁵ Stoeva, Z.; Gomez, R.; Gregory, D. H.; Hix, G. B.; Titman, J. J.; Evolution of structure, transport properties and magnetism in ternary lithium nitridometalates $\text{Li}_{3-x-y}\text{Ni}_x\text{N}$, *Dalton Trans.*, 2004, 3093-3097
- ¹⁶ Jesche, A.; Canfield, P.C.; Single crystal growth from light, volatile and reactive materials using lithium and calcium flux, *Phil. Mag.*, 2014, 94, 2372-2402.
- ¹⁷ Niewa, R.; Huang, Z.-L.; Schnelle, W.; Hu, Z.; Kniep, R.; Preparation, Crystallographic, Spectroscopic and magnetic characterization of low-valency nitridometalates $\text{Li}_2[(\text{Li}_{1-x}\text{M}_x)\text{N}]$ with M=Cu, Ni, *Z. Anorg. Allg. Chem.* 2003, 629, 1778-1786
- ¹⁸ Suzuki, S.; Shodai, T.; Yamaki, J.; Electron energy loss spectroscopy of $\text{Li}_{2.6-x}\text{Co}_{0.4}\text{N}$ (x=0.0 and 1.6), *J. Phys. Chem. Solids*, 1998, 59, 331-336.
- ¹⁹ Bach, S.; Pereira-Ramos, J.P.; Ducros, J.B.; Willmann, P.; Structural and electrochemical properties of layered lithium nitridocuprates $\text{Li}_{3-x}\text{Cu}_x\text{N}$, *Solid State Ionics*, 2009, 180, 231-235
- ²⁰ Ducros, J.B.; Bach, S.; Pereira-Ramos, J.P.; Willmann, P.; Comparison of the electrochemical properties of metallic layered nitrides containing cobalt, nickel and copper in the 1V-0.02V potential range, *Electrochem. Comm.*, 2007, 9, 2496-2500
- ²¹ Gregory, DH; O'Meara, PM.; Gordon, AG.; Hodges, JP.; Short, S.; Jorgensen, JD.; Structure of lithium nitride and transition-metal-doped derivatives, $\text{Li}_{3-x-y}\text{M}_x\text{N}$ (M=Ni,Cu): a powder neutron diffraction study, *Chem. Mater.*, 2002, 14, 2063-2070
- ²² Gordon, A.G.; Smith, R.I.; Wilson, C.; Stoeva, Z.; regory, D.H.; Crystal growth, defect structure and magnetism of new Li_3N -derived lithium nitridocobaltates, *Chem. Comm.*, 2004, 2812-2813
- ²³ Badot, J.C.; Panabière, E.; Emery, N.; Dubrunfaut, O.; Bach, S.; Pereira-Ramos, JP.; Percolation behaviors of ionic and electronic transfers in $\text{Li}_{3-2x}\text{Co}_x\text{N}$, *Phys. Chem. Chem. Phys.*, 2019, 21, 2790-2803.

- ²⁴ Stoeva, Z.; Jäger, B.; Gomez, R.; Messaoudi, S.; Ben Yahia, M.; Rocquefelte, X.; Hix, G.B.; Wolf, W.; Titman, J.J.; Gautier, R.; Herzig, P.; Gregory, D.H.; Crystal chemistry and electronic structure of the metallic lithium ion conductor, LiNiN, *J. Am. Chem. Soc.* 2007, 129, 1912-1920
- ²⁵ Stoeva, Z.; Gomez, R.; Gordon, A.G.; Allan, M.; Gregory, D.H.; Hix, G.B.; Titman, J.J.; Fast lithium ion diffusion in the ternary layered nitridometalate LiNiN, *J. Am. Chem. Soc.* 2004, 126, 4066-4067
- ²⁶ Stoeva, Z.; Smith, R.I.; Gregory, D.H.; Stoichiometry and defect structure control in the ternary lithium nitridometalates $\text{Li}_{3-x-y}\text{Ni}_x\text{N}$, *Chem. Mater.* 2006, 18, 313-320.
- ²⁷ Klatyk, J.; Höhn, P.; Kniep, R.; Crystal structure of pentalithium tris[nitridolithiate/niccolate], $\text{Li}_5[(\text{Li}_{1-x}\text{Ni}_x)\text{N}]_3$ ($x=0.77$), *Z. Krist. NCS*, 1998, 213, 31
- ²⁸ Barker, M.G.; Blake, A.J.; Edwards, P.P.; Gregory, D.H.; Hamor, T.A.; Siddons, D.J.; Smith, S.E.; Novel layered lithium nitridonickelates; effect of Li vacancy concentration on N co-ordination geometry and Ni oxidation state, *Chem. Comm.* 1999, 1187-1188
- ²⁹ Larson, A. C.; Von Dreele, R. B.; *General Structure Analysis System (GSAS)*. Technical Report No. LAUR86-748; Los Alamos National Laboratory, 2004.
- ³⁰ Toby, B.; EXPGUI, a graphical user interface for GSAS. *J. Appl. Crystallogr.* 2001, 34, 210-213.
- ³¹ Mayer, M.; SIMNRA, a simulation program for the analysis of NRA, RBS and ERDA. In: Duggan JL and Morgan IL, editor. Proceedings, 15th international conference on the application of accelerators in research and industry. *AIP conference proceedings* 1999, 475, 541
- ³² Moreau, C.; Mesures et modélisation de réactions nucléaires induites par ions légers d'énergie comprise entre 0.300 et 3.75 MeV, PhD Thesis 2000, Paris VII University, France.
- ³³ Fasoli, U.; Silverstein, E. A.; Toniolo, D.; Zago, G.; The elastic scattering of protons by 6 in the energy range (1.3-5.6)MeV, *Nuevo Cimento* 1964, 19, 1832
- ³⁴ Paneta, V.; Kafkarkou, A.; Kokkoris, M.N.; Lagoyannis, A.; Differential cross-section measurements for the $7\text{Li}(p,p0)7\text{Li}$, $7\text{Li}(p,p1)7\text{Li}$, $7\text{Li}(p,\alpha0)4\text{He}$, $19\text{F}(p,p0)19\text{F}$, $19\text{F}(p,\alpha0)16\text{O}$ and $19\text{F}(p,\alpha1,2)16\text{O}$ reactions, *J. Nucl. Instrum. Met. Phys. Res. B* 2012, 288, 53-59
- ³⁵ Laurat, M.; Rept. Centre d'Etudes Nucleaires, Saclay Reports 1969 No.3727
- ³⁶ Gurbich, A.F.; SigmaCalc recent development and present status of the evaluated cross-sections for IBA, *J. Nucl. Instrum. Met. Phys. Res. B* 2016, 371, 27-32
- ³⁷ Hu, C.H.; Yang, Y.; Zhu, Z. Z.; Structural stability and electronic properties of LiNiN, *Solid Stat. Comm.* 2010, 150, 669-674
- ³⁸ Zunger, A.; Wei, S.-H.; Ferreira, L. G.; Bernard, J. E.; Special quasirandom structures, *Phys. Rev. Lett.* 1990, 65, 353-356
- ³⁹ van de Walle, A.; Tiwary, P.; de Jong, M.; Olmsted, D. L.; Asta, M.; Dick, A.; Shin, D.; Wang, Y.; Chen, L.-Q.; Liu, Z.-K.; Efficient stochastic generation of special quasirandom structures, *Calphad* 2013, 42, 13-18
- ⁴⁰ Kresse, G.; Furthmüller, J.; Efficient iterative schemes for ab initio total-energy calculations using a plane-wave basis set, *Phys. Rev. B* 1996, 54, 11169-11186
- ⁴¹ Kresse, G.; Joubert, D.; From ultrasoft pseudopotentials to the projector augmented-wave method, *Phys. Rev. B* 1999, 59, 1758-1775
- ⁴² Perdrew, J. P.; Ernzerhof, M.; Burke, K.; Rationale for mixing exact exchange with density functional approximations, *J. Chem. Phys.* 1996, 105, 9982-9985
- ⁴³ Monkhorst, H. J.; Pack, J. D.; Special points for Brillouin-zone integrations, *Phys. Rev. B* 1976, 13, 5188-5192
- ⁴⁴ Henkelman, G.; Arnaldsson, A.; Jonsson, H.; A fast and robust algorithm for Bader decomposition of charge density, *Comp. Mat. Sci.* 2006, 36, 354-360
- ⁴⁵ Parlinski, K.; Li, Z. Q.; Kawazoe, Y.; First-principles determination of the soft mode in cubic ZrO_2 , *Phys. Rev. Lett.* 1997, 78, 4063-4066
- ⁴⁶ Togo, A.; Tanaka, I.; First principles phonon calculations in materials science, *Scripta Mat.* 2015, 108, 1-5
- ⁴⁷ Jeynes, C.; Colaux, L.; Thin depth profiling by ion beam analysis, *Analyst* 2016, 141, 5944-5985
- ⁴⁸ Panabièrre, E.; Emery, N.; Bach, S.; J.-P. Pereira-Ramos, JP.; Willmann, P.; Investigation of the chemical stability of Li_7MnN_4 in air, *Corr. Sci.* 2013, 77, 64-68
- ⁴⁹ Panabièrre, E.; Emery, N.; Bach, S.; J.-P. Pereira-Ramos, JP.; Willmann, P.; Chemical stability of layered lithium cobalt nitrides in air, *Corr. Sci.* 2012, 58, 237-241
- ⁵⁰ Pruvost, S.; Berger, P.; Hérold, C.; Lagrange, P.; Nuclear microanalysis: An efficient tool to study intercalation compounds containing lithium, *Carbon*, 2004, 42, 2049-2056
- ⁵¹ Cahen, P.; El Hajj, I.; Speyer, L.; Berger, P.; Medjahdi, G.; Lagrange, P.; Lamura, G.; Hérold, C.; Original synthesis route of bulk binary superconducting graphite intercalation compounds with strontium, barium and ytterbium, *New J. Chem.*, 2020, 44, 10050-10055

-
- ⁵² Brown, I.D.; Recent developments in the methods and applications of the Bond Valence model, *Chem. Rev.* 2009, 109, 6858–6919
- ⁵³ Gagné, O.C.; On the crystal chemistry of inorganic nitrides: crystal-chemical parameters, bonding behavior, and opportunities in the exploration of their compositional space, *Chem. Sci.* 2021,12, 4599-4622
- ⁵⁴ Shannon, R. D.; Revised effective ionic radii and systematic studies of interatomic distances in halides and chalcogenides, *Acta Cryst.* 1976, A32, 751-767
- ⁵⁵ Wu, S.; Neo, S. S.; Dong, Z.; Boey, F.; Wu, P.; Tunable ionic and electronic conduction of lithium nitride via phosphorus and arsenic substitution: a first-principles study, *J. Phys. Chem. C* 2010, 114, 16706-16709
- ⁵⁶ Wu, S.; Dong, Z.; Wu, P.; Boey, F. ; Effect of the transition metal (M = Co, Ni, Cu) substitution on the electronic structure and vacancy formation of Li₃N, *J. Mater. Chem.* 2011, 21, 165-170